Towards airflow sensors with energy harvesting and wireless transmitting properties

Tomasz Blaszczyk[1*], John Aa. Sørensen[1*], Per Lynggaard[2*], Kristian Larsen[3*]

[1]*CWSA, DTU Diplom, Technical University of Denmark, Ballerup, Denmark*
[2]*CMI, Aalborg University Copenhagen, Copenhagen, Denmark*
[3]*Novitek Solutions ApS, Copenhagen, Denmark*

[*]Corresponding author.

DOI: 10.5185/amlett.2018.1925
www.vbripress.com/aml

Abstract

The rapidly growing demand for even more detailed low-cost measurements of weather and environmental conditions, including wind flow, asks for self-sustained energy solutions that eliminate the need for external recharge or replacement of batteries. Today's wind measurement market is limited to traditional anemometers, ultrasonic measurement or expensive LIDAR (Light Imaging, Detection and Ranging) systems. This paper presents the initial design considerations for a low-cost combined air speed and wind direction sensor, which harvests energy to drive it and to power the wireless transmission of system configurations and measurements. An energy-budget for this transmission is included. Copyright © 2018 VBRI Press.

Keywords: Low-cost airflow sensor, aerodynamics, fluid mechanics, energy harvesting, smart materials, piezo paint, oscillations.

Introduction

The demand for smart sensor system with energy harvesting in airflow measurement is huge. Especially in meteorological and related IoT (Internet of Things) applications, where nowadays most popular flow measurement devices are ultrasonic wind sensors. They consume power in range of 37 mA typ. at 24 V (incl. both sensors – wind direction & speed) [**1**]. In this paper we present novel construction of flow sensor able to measure flow speed & direction as well reveal energy harvesting capability for a purpose of measurement sampling and wireless data transmission.

Related works

One of the most demanding constraints in the IoT development is the device energy source.

In the following, examples on energy harvesting systems are presented. So far the authors of this paper are not aware of a publication describing the objective of this paper which is measuring the wind speed and direction, and simultaneously harvest energy from the wind, such that the measurement results can be transmitted wirelessly through e.g. a sensor network using a prescribed transmission duty cycle dependent of the amount of energy harvested. A paper from S. Basagni, et al. [**2**] presents an overview of a selection of energy harvesting methods combining the primary energy source and the sensor applied for energy conversion to electrical power. M. Perez et al. [**3**] presents a selection of small wind-mill electrets based energy harvesters for air-flows in the range of 0.3 meter/sec up to extremely high wind speeds at 340 meter/sec (Mach 1). In the context of the present paper only the lower range of wind-speeds are of relevance. I. Angelo et al. [**4**] presents an example on how to embed an air flow energy harvester in a building design and finally a paper from Cornell University [**5**] shows an idea of a flapping leaf tree structure, which through the use of piezo materials, can be used for harvesting, if placed in a wind flow.

The concept and the challenges

In this work we present developments towards an omnidirectional airflow sensor for measuring wind speed and direction. We are proposing means of integrating piezo electric elements to allow energy harvesting the vortex shedding induced oscillations. The context for this work is limited to simulation for proper sensor flow construction in order to achieve good efficiency in energy harvesting and signal conditioning and provide amount of harvested power for RF transmission.

The idea is a flow sensor that can harvest energy from the phenomena of vortex-induced vibrations & vortex shedding physics. Steady flow around an object, such as a half cylinder, induce unsteady separation and vortices downstream. The characteristic flow pattern

shows oscillating clock-wise and anti-clock wise vortices, known as "Kármán Vortex Street", as described by Von Karman. This physics allows us to construct pairs of flaps where main task is to harvest energy from oscillations. However, since the vortex dynamics varies with increasing flow speed, the energy harvesting must be carefully optimized. It makes a huge impact where energy is converted into turbulent flow and wakes.

The "half cylinder" system enables energy conversion from laminar into turbulent. Furthermore increasing the incident flow will add energy to the system. This energy will drive the mechanical harvesting beams covered with piezoelectric powder paint.

We have carried out CFD modelling with airflows spanning from 1-15 m/s. At this flow speed the airflow is dominated by a laminar vortex street reaching into a transition range with turbulence in vortex. In this region the laminar flow in contact with an object with an appropriate Reynolds number (Re ~ 50 to 20000) has the ability to generate aerodynamic lift oscillation acting on object. In order to visualize and achieve best construction to sensor performance including energy harvesting a set of simulation models has been created and analysed using Comsol Multiphysics. To achieve suitable Reynolds number for surrounding low velocity flow, and be able to sense flow in all direction a special omnidirectional sensor construction is created **Fig. 1**.

The sensor is composed of several particular sensor modules encapsulated in a wing profile – "doughnut sandwich". In our-study we focus only on snipped of the sensor that will reveal and present essential omnidirectional sensor functionality and exhibit overall sensor performance. Omnidirectional sensor composed from set of such sensor subparts is presented in **Fig. 2** with violet colour.

The essential part of the sensor construction is build up from a half cylinder of 1cm radius and 2 beams with different geometry configuration. **Fig 3.** Presents beams with length of 3 cm each but different configurations has been studies where the main aim was to achieve good energy harvesting results and flow sensitivity.

The front beam joined with the half cylinder is acting as the main energy harvester unit, whereas second beam is more elastic and responsible for good sensor sensitivity when wind speed is lower than 1m/s. The half cylinder shape is intended to be the main vortex shedding generator, initiating oscillating flow that affects the whole structure downstream. The half cylinder is movable, only fixed at the round end of the beam. Similarly the second beam is fixed at the round end and can oscillate in synergy with the vortex flow.

In order to find good geometry parameters for the second beam (position, length, height, material properties) and the overall omnidirectional sensor a basic model has been created which contains only one beam combined with half-cylinder **Fig. 4.**

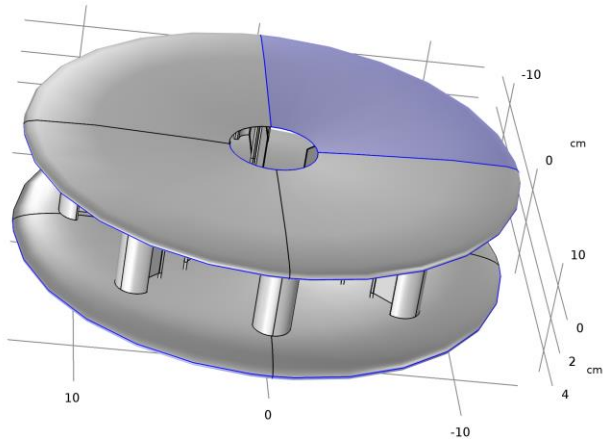

Fig. 1 Omnidirectional construction of the sensor.

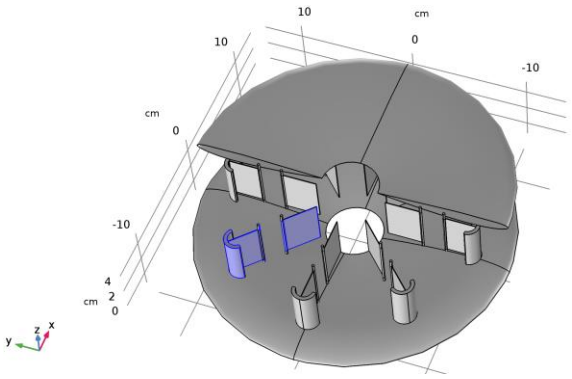

Fig. 2. Essential (studied) part of sensor construction selected with violet colour.

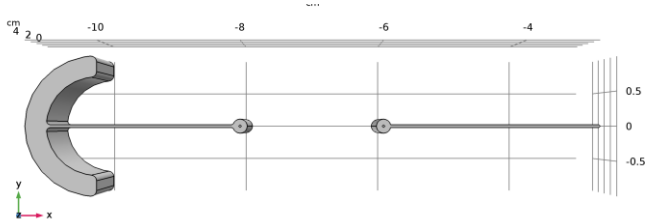

Fig. 3. Sensor geometry – top overview. Wind direction in model is from left to right. Thickness of the beam is typically 0.4 mm. The structures are freely moving only constrained at the round anchor points at x=-6 and x=-8cm.

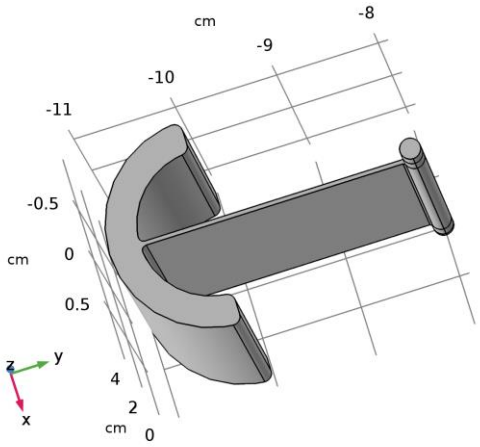

Fig. 4. Beam with half cylinder.

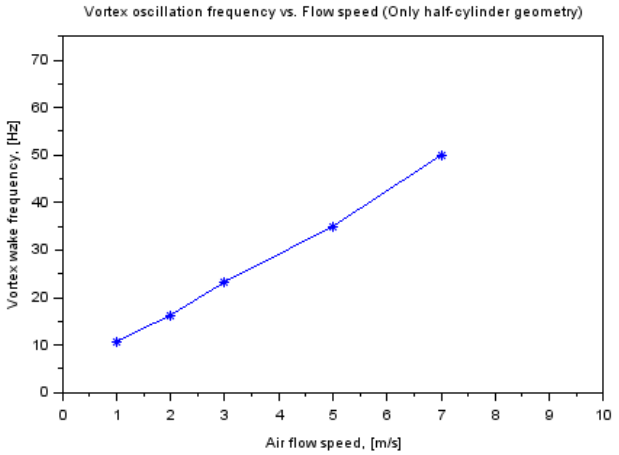

Fig. 5. Vortex oscillation frequency vs flow speed.

Vortex shedding properties of half-cylinder bluff body

This model, also used for power calculation in paragraph IV, helps to determine the frequency of vortex shedding (wake frequency) of the system together with other parameters [**6**] shown in **Table T1**. Assuming this part acts as "independent" vortex generator and dictates the overall frequency of the whole system **(Fig. 5).**

Table 1. Flow speed *vs* vortex oscillations.

Flow speed [m/s]	Osc. Freq.[1/s]	Re (@20C)	Strouhal number
1	10.8	1324	0.22
2	16.3	2647	0.16
3	23.2	3971	0.15
5	35	6618	0.14
7	50	9265	0.14
10	70 (est.)	13235	0.14 (est.)
15	105 (est.)	19853	0.14 (est.)

Mechanical analysis

The natural frequency of the mechanical structure for the half cylinder with beam model has been found **(Fig. 6).** Tuning of the performance of the sensor device is a matter of finding optimal combination of the dynamic structural properties, especially the natural frequencies, and the flow dynamic properties mainly related to the vortex oscillating frequencies. The exact combined aero elastic behaviour is however difficult to predict without careful flow simulations. An exact match of vortex and mechanical resonance frequencies will allow substantial input of energy into the mechanical structure, but will easily lead to uncontrolled vibrations, instability and collapse. An optimal balance is needed.

Mechanical structure reveals resonant frequencies and vibration modes for first half-cylinder bluff body **Fig. 6 (a) & (b).**

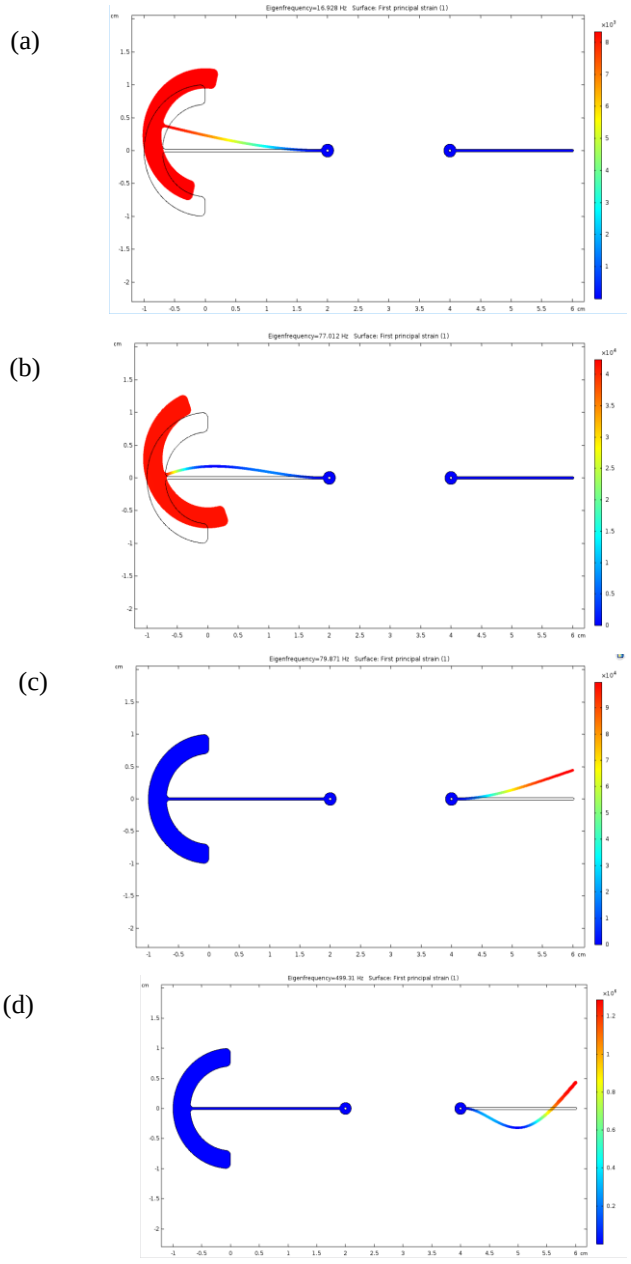

Fig. 6. Natural frequencies and vibration modes: 16Hz, 77 Hz, 79Hz & 499Hz (a) Half-cylinder 1st vibration mode at 16.9Hz (b)Half-cylinder 2nd vibration mode at 77.0 Hz (c) Second flap element, 1st vibration model at 79.9Hz (d) Second flap element, 2nd eigen mode at 499.3Hz.

The first 4 vibration modes are shown in **Fig. 6**. With this sensor design it is possible to tune the resonance frequencies by adjusting the length and thickness of the suspension beams.

First beam with cylinder is made of elastic material with parameters presented in **Table 1**. Where second beam is more elastic defined by parameters shown in **Table 2**.

Table 2. Material parameters for beam with cylinder.

Name	Value	Unit
Density	1150[kg/m^3]	kg/m³
Young's modulus	900[MPa]	Pa
Poisson's ratio	0.48	1

Table 3. Material parameters for second beam.

Name	Value	Unit
Density	1000[kg/m^3]	kg/m³
Young's modulus	100[MPa]	Pa
Poisson's ratio	0.40	1

Simulation results for complete sensor element

Finally, together with the second beam combined results are provided in **Fig. 7** for a range of wind speed parameter (1, 3, 5 m/s) using simulation environment **Fig. 8**.

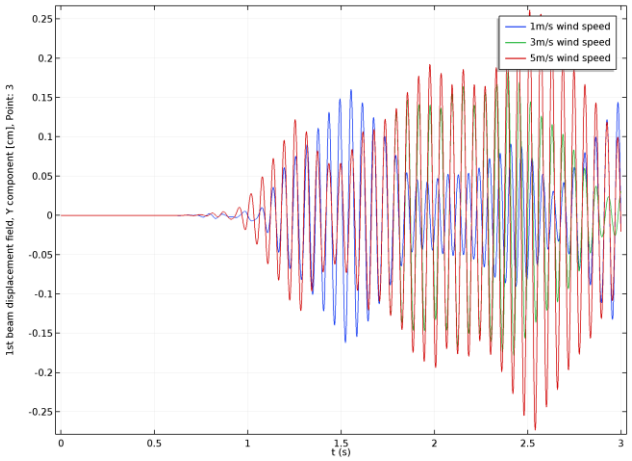

Fig. 7. First beam displacement for speed: 1m/s (blue), 3m/s (green), 5m/s (red)

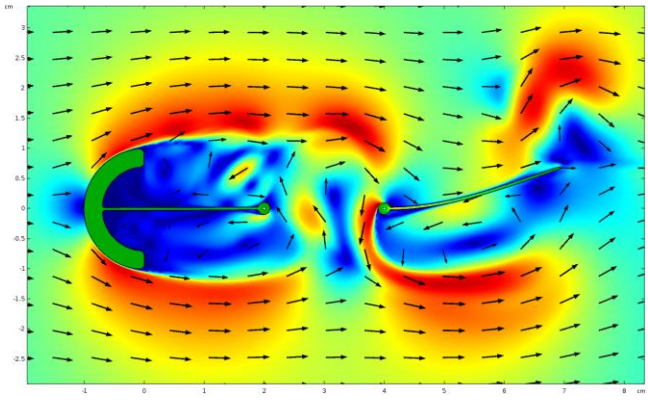

Fig. 8. Simulation model in Comsol Multiphysics. Sensor construction – With 2 harvesting beams, here at 2m/s inflow speed.

It is noted that higher speed of flow starts oscillation faster, with amplitude increasing slower compare to lower wind speed (i.e.:1m/s)

Fig. 9 presents sensor beam deflection at frequency of 16Hz for first beam which match natural resonant frequency of beam and tend to be good energy harvester and exhibits good sensitivity. Increasing or decreasing flow speed will locked-in to natural frequency of the half cylinder with beam **Fig. 7** causing good energy transfer to the beam at natural frequency. Second shorter beam has higher natural frequency 79Hz **Fig. 6** which is well sensitive for velocities above 15m/s). This has to be study in more details.

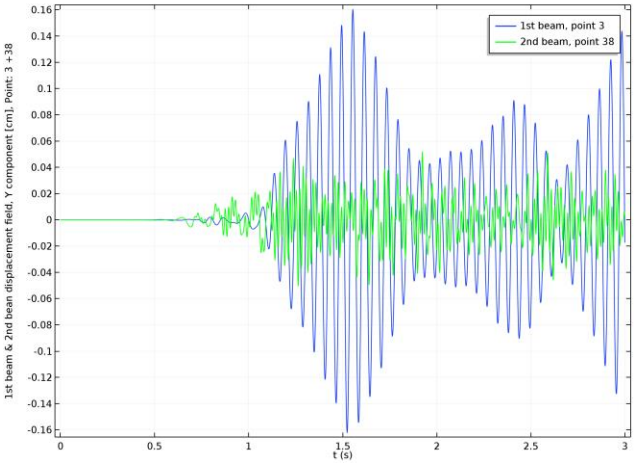

Fig. 9. Sensor's two beams deflection – blue color: first beam with cylinder; green colour –second beam. Dominating vibration frequency of 1st beam is 16Hz (blue) and for second beam 79Hz (green).

We see clear oscillations already at 1 m/s. According to the vortex frequency analysis, the oscillation frequency and mechanical eigenfrequency is estimated to be equal at about 2m/s flow speed. In this way the sensitivity of the device is enhanced at the lower end of the flow velocity range.

Further tuning of mechanical eigenfrequencies and the vortex frequency is needed to further optimize the device sensitivity and maximize energy absorption.

A study of the pressure gradients of a 3 dimensional sphere revealed best position for beams for energy harvesting.

Details on the computational fluidic dynamic (CFD) simulations

Fluid flow presented in our study is described by 3 main equations: (I) the Navier-Stokes Equations:

$$\rho\left(\frac{\partial u}{\partial t} + (u \cdot \nabla)u\right) = -\nabla p + \nabla \cdot \left[\mu\left(\nabla u + (\nabla u)^T - \frac{2}{3}(\nabla \cdot u)I\right)\right] + F$$

where ρ is fluid density $[kg/m^3]$ and μ is fluid dynamic viscosity $[Pa \cdot s]$. Both ρ & μ represents material properties. u is fluid velocity and p is fluid pressure . First part correspond to inertial forces, $-\nabla p$ to pressure forces, $\left[\mu\left(\nabla u + (\nabla u)^T - \frac{2}{3}(\nabla \cdot u)I\right)\right]$ to viscous forces and F to external forces applied to the fluid.

(II) Conversion of mass (continuity equation):

$$\frac{\partial \rho}{\partial t} + \nabla \cdot (\rho u) = 0$$

(III) Equation of state represented by pressure, temperature & density

$$\rho = \rho(p, T)$$

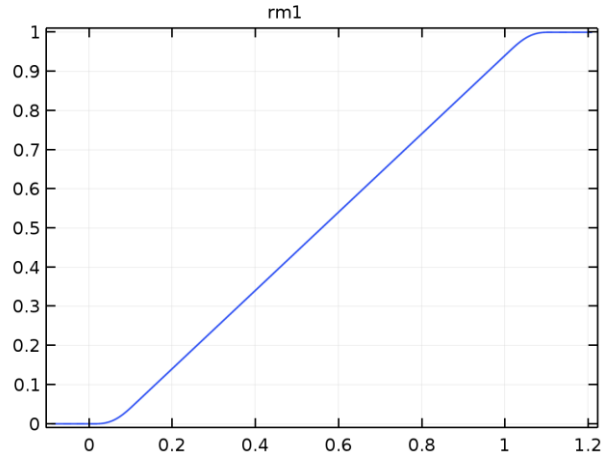

Fig. 10. Ramp-up function for inflow speed

Our model in fluid flow governed by the Navier-Stokes equations uses temperature of 293.15[K]. And laminar flow velocity ranging from 1m/s up to 15m/s with ramp show in **Fig. 10,** where inflow is defined as: flowspeed*rm1(t[1/s]).

Based on Reynolds number for predefined conditions the single-phase, laminar flow interface has been chosen where both velocity and pressure are computed.

Finite element CFD simulations have been executed in Comsol Muliphysics software **(Fig. 10)** with Direct solver performing LU-decomposition for solving linear system. The flow is here modelled using a 2D time-dependent flow simulation, using a laminar flow model and a fluid-structure interaction model with non-fixed geometry (ALE) allowing large non-linear deformation of mechanical elements. The simulations were initiated with a smooth ramp-up function **(see Fig. 9)** of the flow velocity from 0 to the nominal speed to help converges of the simulations. This method proved overall successful.

An energy harvesting construction

To substantiate the process of harvesting energy from the forces provided by the vortexes in a turbulent airflow a simulator has been designed and constructed. It is able to calculate the output power in a specified load resistance for an applied input force which is provided by flowing air. The key element in this simulator is two sets of equations. The first set describes the mechanical behaviour and parameters for the energy harvesting beams. The second set describes the transfer of mechanical strain to piezo-elements which harvests and produces the output power. These equations are combined and solved in a simulator for a selected parameter-range to explore the parameters of the beams in terms of the relation between the distributed force and the delivered output power.

In the following subsection A is allocated to explore and elaborate the sets of equations that constitute the simulator and subsection B presents, discusses, and elaborates the outputs and findings from the simulated beams.

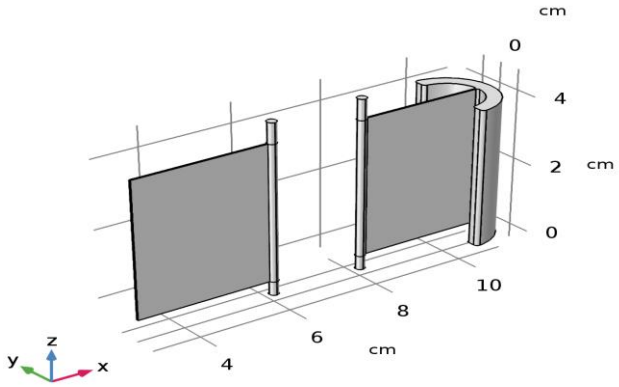

Fig. 11. The mechanical construction of the vortex-induced energy harvester used for simulations in this work.

A simulation model

As discussed, the mechanical model used for the simulations handles vortex-induced vibrations. It consists of two harvesting parts **(Fig. 11).** The first part is constructed as a half-cylinder, i.e. a bluff body with a mounted harvesting beam that is coated with a thin layer of piezo-paint. The second part is a beam positioned in line with the first one, but with a small offset to this **(Fig. 11).** Similarly, the second beam is coated with a thin layer of piezo-paint.

To simplify the mechanical model for these harvesting beams (Fig. 11) their mechanical properties is modeled as two cantilever beams where the transferred forces from the vortexes are approximated by adding forces to the beams **(Fig. 12)**. The beam marked "beam-1" models the beam with the bluff body. Because the bluff body is the primary force on the beam it is modeled by adding one point force at the end of the beam (Fig. 11). Similarly, "beam-2" models the second beam (Fig. 11) where the forces from the vortexes are modeled as distributed forces acting along the beam **(Fig. 12).**

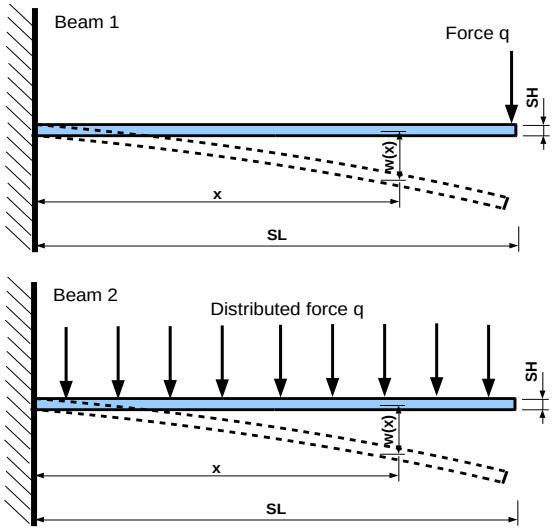

Fig. 12. Model of the harvesting beams. "Beam-1" is the forces transferred from the bluff body modeled as a point force. "Beam-2" models the vortexes as distributed forces along the beam. The deflection of the beams at distance x is w(x) and the beam parameters are length S_L and thickness S_H.

From the deflection w(x) of the beams **(Fig. 12)** it is possible to calculate the strain on the beams at position x [*7*]. This strain depends on the thickness of each of the beams S_H (which is different for beam 1 and 2) and the double derivative of the deflection w(x) as shown in equation 1.

$$\varepsilon(x) = \frac{S_H}{2}\frac{d^2 w(x)}{dx^2} \tag{1}$$

Where:

S_H – beam height (thickness) for beam 1 or 2

w(x) – deflection of the beam at distance x (fig 12)

The transfer function between input strain and output current from the piezo element is [*8*]:

$$i(t) = -\int_{x=0}^{L} d_{31} Y_p P_W \frac{\partial}{\partial t}\left(\frac{\partial^2}{\partial x^2}\frac{S_H}{2} w(x,t)\right)dx - \frac{\varepsilon_{33}^S P_W P_L}{P_H}\frac{dv(t)}{dt} \tag{2}$$

Where:

i(t) – Piezo current at the terminals

v(t) – Piezo voltage at the terminals

d31 – Piezoelectric constant

Yp – Young's modulus for the piezo element

PW, PH, PL Piezo: width, height, length

w(x,t) – deflection as a function distance and time

ε33 – Permittivity of piezo element

It is observed that the first term in equation 2 is the time derivative of the strain multiplied by constants which change its dimension to current. Similarly, the last part of the equation which includes the permittivity can be modeled as a capacitor (C_p). By using these observations equation 2 can be written (3):

$$i(t) = -d_{31} Y_p P_W \frac{\partial}{\partial t}\int_{x=0}^{L} \varepsilon(x,t)dx - C_p \frac{dv(t)}{dt} \tag{3}$$

Where:

Cp – capacity of the piezo element

Focusing on the parameters in equation 3 it is noted that this can be modeled as a Norton current source in parallel with the capacitor Cp as illustrated in **Fig. 13**.

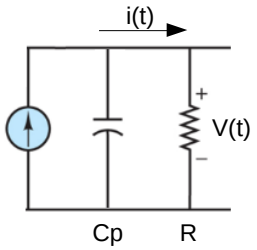

Fig. 13. Electric equivalent-model for a piezo element with an external load resistor (R).

Writing the governing equation for the equivalent model (fig 13), solve it with respect to the steady-state response v(t), and substitute the terms from equation 3 yields (4):

$$i_g(t) = \frac{v(t)}{R} + C_p\frac{dv(t)}{dt}$$
$$v(t) = \frac{-d_{31} Y_p P_W \frac{\partial}{\partial t}\int_{x=0}^{L}\varepsilon(x,t)dx}{\frac{1}{R} + j\omega C_p} \tag{4}$$

Where:

R – Load resistor (receiving the harvested power)

A transfer function that maps the strain into voltage can be found by dividing equation 4 by the average strain from equation 1 which yields (5):

$$\bar{\varepsilon}(t) \equiv \frac{1}{S_L}\int_{x=0}^{L}\varepsilon(x,t)dx$$
$$H(t) = \frac{v(t)}{\bar{\varepsilon}(t)} = -\frac{d_{31} Y_p P_W S_L \frac{\partial}{\partial t}\bar{\varepsilon}(t)}{\left(\frac{1}{R} + j\omega C_p\right)\bar{\varepsilon}(t)} \tag{5}$$

By multiplying the transfer function (5) with the average stains from the bending of the beams caused by the vortexes it is possible to find the output voltage and thereby the delivered power to resistor R from each of these beams. This strain can be calculated by rewriting equation 1 in terms of a bending moment equation and integrate the result to find the average strain (6) for each of the beams. Similarly, the time dimension is added by letting the beams oscillate in the first mode of their resonance angular frequencies.

$$Beam-1:$$
$$\bar{\varepsilon}(t) \equiv \frac{1}{S_L}\int_{x=0}^{S_L}\varepsilon(x,t)dx$$
$$= \frac{1}{S_L}|q_{\max}|e^{j\omega t}\int_{x=0}^{S_L}\frac{S_H}{YsIs}\left(-q(t)S_L + q(t)x\right)dx$$
$$= -\frac{S_H S_L}{4YsIs}|q_{\max}|e^{j\omega t} \equiv |\varepsilon_{\max}|e^{j\omega t}$$
$$Beam-2:$$
$$\bar{\varepsilon}(t) \equiv \frac{1}{S_L}\int_{x=0}^{S_L}\varepsilon(x,t)dx \tag{6}$$
$$= \frac{1}{S_L}|q_{\max}|e^{j\omega t}\int_{x=0}^{S_L}\frac{S_H}{YsIs}\left(\frac{-q(t){S_L}^2}{2} + q(t)S_L x - \frac{q(t)x^2}{2}\right)dx$$
$$= -\frac{S_H {S_L}^2}{6YsIs}|q_{\max}|e^{j\omega t} \equiv |\varepsilon_{\max}|e^{j\omega t}$$

Where:

q_{max} – Maximum distributed force

ω – Angular frequency

Y_s – Young's modulus for the beam

I_s – Moment of inertia for the beam

Multiplying the average strain equation 6 with the transfer function equation 5 yields the voltage and power outputs (7):

$$Beam-1:$$

$$v(t) = -\frac{j\omega d_{31} Y_p S_W}{\left(\frac{1}{R} + j\omega C_p\right)} \frac{S_H S_L^{\,3}}{6YsIs} |q_{\max}| e^{j\omega t}$$

$$Beam-2:$$

$$v(t) = -\frac{j\omega d_{31} Y_p S_W}{\left(\frac{1}{R} + j\omega C_p\right)} \frac{S_H S_L^{\,2}}{4YsIs} |q_{\max}| e^{j\omega t} \quad (7)$$

$$P_{R,ave}(t) = \frac{|v(t)|^2}{2R}$$

By using the harvested power (7) in Friis transmission formula [9] [6] a link budget can be calculated (8). In this equation it is assumed that the power used by the transmitter is constant in a transmission time window ΔT_t. This power is harvested in the time window from T_0 to T_1 (8).

$$P_{t,av} = \frac{\int_{T0}^{T1} P_{R,ave}(t)dt}{\Delta T_t} \quad (8)$$

$$P_r = G_r G_t \left(\frac{\lambda}{4\pi R}\right)^2 (\eta_t P_{t,av} - L_t)$$

Where:

Pr - Received power with antenna gain Gr

Pt - Transmitted power with antenna gain Gt

λ - Wavelength of the signal

R - Distance between receiver and transmitter.

η_t – Transmitter efficiency

ΔT_t- Transmit time for one data frame.

Lt – Other losses see [*10*].

Elaborated simulation results

This section presents and elaborates the simulated results for the harvested power from the beams used in this work (Fig 11). Each of these beams is a composition of a plate with a thin layer of piezo-paint [*11*]. The mechanical data for these beams are presented in **Table 4**.

Table 4. Values used for the simulations.

Parameter	Value	Description
Beam-1: S_H, S_W, S_L	0.8,40,30	Beam dimensions[mm]
Beam-2: S_H, S_W, S_L	0.8,40,20	Beam dimensions[mm]
Beam-1: Ys Beam-2: Ys	900 100	Young's modulus for the beam [MPa]
d31	15	Piezoelectric constant [pm/V]
ε33	15	Permittivity of piezo element [nF/m]
Yp	29	Young's modulus for the piezo element [GPa]

By relating equation 6 and 7 it is clear that the time changes of the strain can be seen as the main generator in an energy harvesting system based on a piezoelectric effect. Elaborating over the value of the strain in beam-1 it can be calculated by dividing equation 6 with S_H, integrating it twice, and providing the necessary boundary conditions **(Fig 14)**.

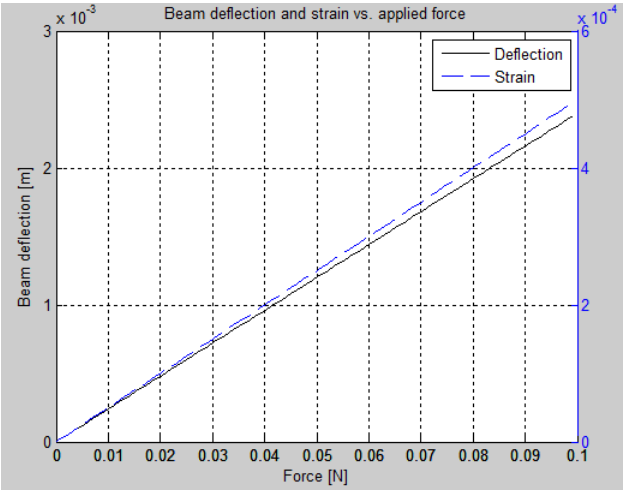

Fig. 14. Deflection and average strain of beam-1 as a function of the applied point-force.

By using curve-fitting it is possible to model the square of the envelope for the deflection of beam-1 (Fig. 9). The square-root of the average of this deflection can then be used to find the maximal equivalent point-force (q_{max} equation 6) by performing a double integration of ε(x,t) with respect to x in equation 6. For beam-1 this value is an approximately deflection of 0.9 mm which from fig 14 yields a point-force of approximately 38 mN and a strain of approximately 0.19 mN/m^2. Similarly, for beam-2 the strain is 0.125 mN/m^2.

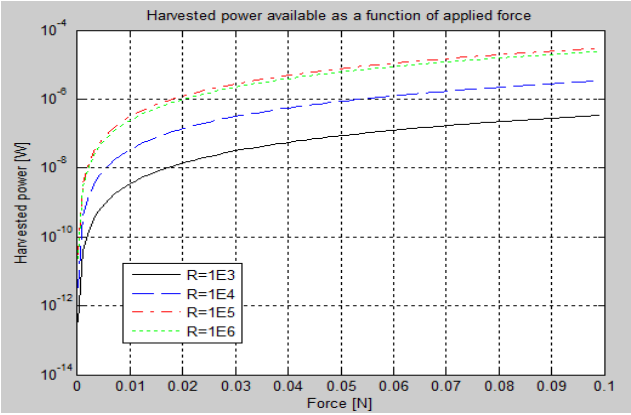

Fig. 15. Harvested power from beam-1 as a function of applied point-force. The four plots represent different load resistor values and the frequency of the time varying force is 16 Hz.

The harvested average power from beam-1 can be calculated by using beam-1 mode one resonance of 16 Hz (Fig 5) and equation 7 which is plotted **(Fig 15)**. From this figure the harvested power is approximately 7 μW in a load resistor (R) of approximately 100 kΩ. Similarly, beam-2 with mode 1 resonance at 34 Hz yields approximately 3 μW in a load resistor (R) of approximately 100 kΩ.

As observed **(Fig. 15),** the harvested power is a function of the load resistance (R) of the circuit. This is the case because the complex output impedance for the transfer function must match the load resistance for maximal power transfer.

To optimize the power output from the beam the input force generated by the vortexes in the airflow must be increased to increase the strain; however, the strain must be inside the "plastic deformation" range of the material to prevent it from breaking. Another factor that limits the maximal harvested power is the theoretical available mechanical energy in an airstream ("aero-electro-mechanical" efficiency). This can be calculated for the beams used in this work by assuming the flow is stationary [*7*] **(Fig. 16).** It is noted that the y-axis is logarithmic which actually hides the fact that the maximal harvested power is a linear function of the beam deflection.

The "aero-electro-mechanical" efficiency of a beam harvester is a non-linear function of its working point. However, for beam-1 it can be approximated as the power output of 7 μW divided by the mechanical power available from the air flow which is 43 μW **(Fig. 16)**. This yields an "aero-electro-mechanical" efficiency of approximately 16 percent, which is acceptable compared to similar research [*12*].

As discussed, this selected beam construction has a dual function because it is able to produce power from the vortexes in an air-flow and similarly, act as an airflow-sensor. Exploring equation 7 it is noted that the output voltage is a linear function of the distributed input force if and only if the frequency of the vortexes is constant. However, if the transfer-function from the airflow to the distributed forces acting on the beam is non-linear this

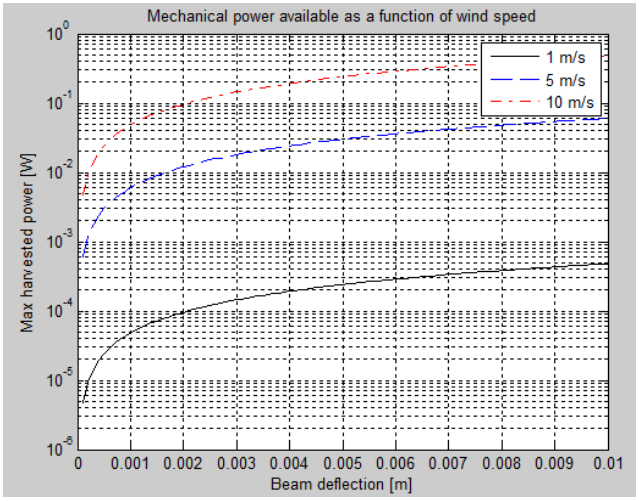

Fig. 16. Mechanical power available as a function of wind speed and beam-1 deflection. Note y-axis is logarithmic.

needs to be compensated. More research is needed to clarify this.

Focusing on the link budget (8) the term $P_{t,av}$ is the harvested power available for the transmitter and sensor electronics in the time window ΔT_t. To quantify this equation an example which is based on the parameters given in [*10*] is elaborated. If it is assumed that the transmitter uses 1 mW ($P_{t,av}$) in 200 mS (ΔT_t) to transmit one frame (a message) and as calculated previously the energy harvester provides 10 μW (7 μW from beam-1and 3 μW from beam-2) in the time window from T_0 to T_1 it is possible to transmit a message approximately every 20 seconds (i.e. T_0-T_1). Likewise, transmitting with 10 mW gives approximately 200 seconds between repeated transmissions and transmitting with 100 mW gives approximately 33 minutes between repeated transmissions. These transmitter power levels are able to provide a useable communication channel as discussed in [*10*] Fig. 8. This figure is reprinted as **Fig. 18**.

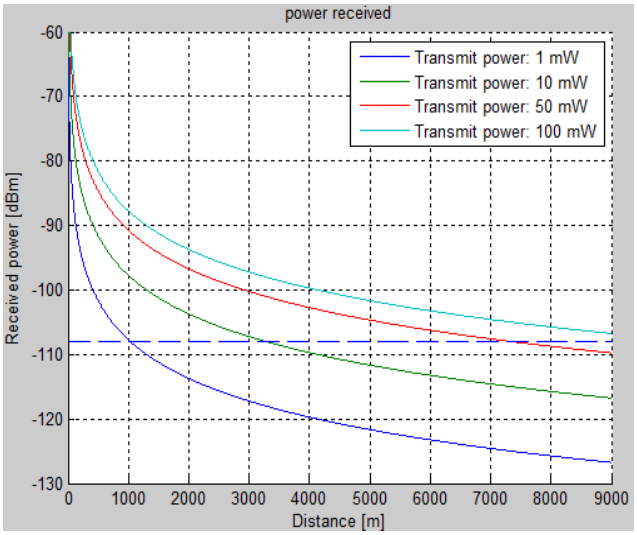

Fig. 18. The received power as a function of transmitted power and distance (a link margin of 12 db is included). The dashed line indicates the receiver sensitity level. This figure is copied from [*10*].

Thus, it is possible to transmit a message every approximately 20 seconds at a distance of 1 km and a message every approximately 33 minutes over a distance of 9 km.

Conclusion

The study has presented a design concept of a smart wind sensor device for combined airflow speed and direction sensing and energy harvesting for wireless connectivity. The sensing element utilizes airflow induced vortex shedding which cause vibrations of mechanical structural elements. The sensor design has been modelled via computational fluidic dynamic simulations yielding dominant vibrations of energy harvesting structures already from 1 m/s and up to 15m/s.

The present design exhibits room for further optimizations in terms tuning mechanical resonance frequencies and the vortex shedding frequency properties to allow a maximum of flow energy to be absorbed into energy harvesting sensor elements.

An energy harvesting principle utilizing piezo electric surface elements has been explored and elaborated using simulation models. These models show the vital parameters in designed sensor construction

Analysis of the electrical power budget has shown results only for small part of omnidirectional sensor. Further studies open future potential applications for such kind of sensors.

Acknowledgements

This work was supported in part by DTU Diplom innovation funds.

References

1. WAC 55. WAC155 - Vaisala Serial Wind Transmitter part of AWS310 Automatic Weather station. [Online]. www.vaisala.com
2. S. Basagni, M.Y. Naderi, C. Petrioli, and D. Spenza, "Wireless Sensor Networks With Energy Harvesting," in *Mobile Ad Hoc Networking: Cutting Edge Directions*.: John Wiley & Sons Inc., Hoboken, NJ, 2012, ch. Chapter 20.
3. M. Perez et al., "A cm scale electret-based electrostatic wind turbine for low-speed energy harvesting applications," *Smart Mater Struct*, no. 25, 2016.
4. I. Angelo, J. Aquino, and B. Hughes, "Integration of aero-elastic belt into the built environment for low-energy wind harnessing: Current status and a case study," in *Energy Conversation and Management*.: Elsevier, 2017.
5. "Flapping leaf generator for wind energy harves-ting," Cornell University, 2009.
6. W. Yeung, "On the Relationships Among Strouhal Number, Pressure Drag, and Separation Pressure for Blocked Bluff-Body Flow," *Journal of Fluids Engineering*, vol. 132, 2010.
7. M. Vable, *Mechanics of Materials*, 2nd ed.: Oxford University Press , 2009.
8. D. Erturk and A. Inman, "A Distributed Parameter Electromechanical Model for Cantilevered Piezoelectric Energy," *Journal of Vibration and Acoustics*, vol. 130, pp. 1-15, 2008.
9. J. Shaw, "Radiometry and the Friis transmission equation ," *American Journal of Physics*, 2013.
10. T Blaszczyk and P Lynggaard. (2015) CWSA. [Online]. www.wirelesscenter.dk
11. MEGGITT A/S. (2017) meggit. [Online]. meggit.com
12. D. Huseyin, N. Akaydın, and A. Yiannis, "Flow-Induced Vibrations for Piezoelectric Energy Harvesting," in *Advances in energy harvesting methods*., 2013, ch. 10, p. 241.

